ASSESSING FLOOD DAMAGES OF THE 1997 ODER FLOOD AND THE 1995 MEUSE FLOOD

A. De Roo [1], J. Van Der Knijff [1,2], M. Horritt [3], G. Schmuck [1], S. De Jong [2,4]
[1] European Commission, Space Applications Institute, Joint Research Centre, TP 262, 21020 Ispra (Va), Italy, ad.de-roo@jrc.it
[2] Department of Physical Geography, Utrecht University, The Netherlands, johan.van-der-knijff@jrc.it
[3] Department of Geography, University of Bristol, United Kingdom, matt.horritt@bristol.ac.uk
[4] Department of GeoInformatics and Remote Sensing, Wageningen Agricultural University, The Netherlands, s.dejong@geog.uu.nl

KEYWORDS: **F**loods, SAR, Meuse, Oder, flood extent, flood damages.

ABSTRACT

Within the floods research activity of the Natural Hazards Project of JRC-SAI, ERS-SAR images are used to detect flooded areas during the July 1997 flood in the Oder catchment and the January 1995 flood in the Meuse catchment. Threel methods are used to obtain the flooded areas from the SAR images: two supervised classification method and the 'snake'-method. The different methods are validated using aerial photographs taken during the flood and classified using field data. Using the information on the flooded areas, overlays are made with high-resolution Digital Elevation Models and Land Cover maps, such as the Corine Land Cover database, to obtain flood depths, land use statistics of the flooded areas, and maps of land use in the flooded area, indicating vulnerable sites such as hospitals or power stations. Also the flood extent maps are compared with flood inundation frequency maps. The flooded areas derived from the SAR images will be in a later stage of the flood project used to validate flooded areas simulated with the physically-based distributed LISFLOOD flood simulation model, developed at SAI/JRC

1. INTRODUCTION

Recently, several regions of the world experienced dramatic flooding. Examples are Bangladesh (1988), Vaison La Romaine (France, 1992), Mississippi River (USA, 1993), Meuse (Netherlands, 1993), Piemonte (Italy, 1994), Rhine and Meuse (Netherlands, Belgium and Germany, 1995), Biescas (Spain, 1996), Oder (The Czech Republic, Poland and Germany, 1997), China (1998) and Central America (1998). Therefore, the Space Applications Institute of the Joint Research Centre has started a flood research programme in support of the Commission policies which are linked to the flood problem. Combined with existing information on land use, soils and topography, maps of the flooded areas provide information that can be used for flood damage assessment, urban and rural planning and validating flood simulation models.

The use of ERS SAR radar imagery for flooded area mapping appears to be very promising. The cloud-penetrating properties of radar data make SAR images much more useful for flood monitoring than e.g. Landsat or Spot data (Portmann, 1997). On a radar image, areas that are flooded usually appear much darker than the non-flooded areas. Thus, maps of flooded areas can be made very quickly, and at much lower costs than using traditional mapping methods. Automatic image classification seems to be the most appropriate technique for deriving flooded areas from radar imagery. Usually, some additional processing has to be carried out on the resulting 'flooded area' maps, because the raw classification results rarely match the end-users' requirements. Standardised, well-established methods for doing this hardly exist. Moreover, this stage of the 'flooded area' mapping usually involves manual editing of the classification results, which is not desirable. Automated, more objective and reproducible methods are needed.

In this paper, the question is addressed how the results of an automatic 'flooded area' image classification can be improved. Any method to do this should -whenever possible- meet the following requirements:

- the method should be –as much as possible- automated
- in order to combine the flooded area maps with auxiliary data (e.g. land use, elevation), it should be easy to implement the method into existing GIS packages (for example Arc/Info).
- instead of manually editing the classification results, the method should use existing information on e.g. topography or the locations of the main rivers.

In this paper two methods are presented that –to a large extent- meet these requirements. These methods were tested and validated using ERS-1 images of the Meuse flood of 1994/1995 and the Oder flood of 1997. The results of the automatic flood delineation were then combined with land cover data to derive land use statistics of the flooded areas. Also, the results were combined with a digital elevation model, in order to investigate the possibility to estimate flooding depths.

2. EXISTING METHODS FOR DERIVING FLOODED AREAS FROM RADAR IMAGERY

In the recent past a variety of methods have been applied to delineate flooded areas on SAR imagery. The simplest method

involves visual interpretation of a SAR image. Flooded areas can be identified because of their darker grey tones. Flood maps can be produced by digitising the flood line on screen. Though perhaps accurate, this method is not feasible because it is very time consuming.

When images are available from different dates, representing the flooded and non-flooded situation, colour composites of 2 or 3 images can be made. In these colour composites, flooded areas are easily identifiable by their bright colours (e.g. Delmeire, 1997). Although this technique is useful for a getting a quick visual view of the flooding extent, the results cannot be easily merged with other GIS data.

Another approach is to use differencing techniques. For example, Badji & Dautrebande (1997) proposed a 'conceptual flood inundation index' (ICN):

$$ICN = K.(DN^2_n - DN^2_i + e)/ (DN^2_n + DN^2_i + e)$$

Where DN_n is the radar backscatter value of the non-flooded image and DN_i is the backscatter value of the flooded image. K is a scaling factor and e is a small constant that prevents any divisions by zero. The value of this index increases as the differences between the DN-values of the two dates become larger. Theoretically, areas that are flooded on one image and non-flooded on the second one should result in very high values of this index. A disadvantage of this method is that it doesn't *directly* identify flooded areas: a certain threshold value has to be determined, above which pixels are to be called 'flooded'. Furthermore, because two different images are needed, more time is needed to pre-process the data (geo-referencing, filtering, etc.).

Supervised image classification provides another way to derive flooded areas. The classification process involves two steps. First, some flooded and non-flooded areas are selected in the radar image. The pixel value distributions of these flooded and non-flooded 'training sites' are then used to classify the image: for each pixel in the image, the probability of belonging to the 'flooded' and 'non-flooded' class is computed. The pixel is then assigned to the class for which it has the highest probability. The advantage of this method is that 'flooded area' maps can be made very quickly. A disadvantage is that the resulting classified image usually contains a large amount of misclassified pixels. The main cause for this is that on a radar image, the flooded areas are relatively inhomogeneous, encompassing a wide variety of grey tones (Oberstadler et al, 1997). Also, forested areas resemble flooded areas on a radar image. The result is that the classified image often contains many small groups of pixels that are misclassified as 'flooded', as well as 'non flooded' gaps within the flooded areas. Correcting for this usually involves various spatial filtering steps, as well as manual editing of the classification results. This can be a time consuming process, and the filtering and editing can have adverse side effects on the accuracy of the resulting flood map. Furthermore, it doesn't provide an objective and straightforward way to mapping flooded areas.

3. IMAGE CLASSIFICATION AND PROCESSING

3.1 Description of the processed ERS scenes

For the 1995 Meuse flood, three ERS-1 SAR scenes were acquired. The southern scene is the Meuse area in France, but it was not used because of its poor quality. The middle scene shows the part of the Meuse catchment from Dinant (Belgian Ardennes) to Roermond. For the major part of this image, the Meuse and its tributaries flow through a narrow valley system in an area of moderate to high relief. This results in layover effects on large parts the radar image, making it impossible to delineate flooded areas. The northern scene (figure 1) shows the northwestern part of the catchment (north of Roermond). The wide, relief-less alluvial plain of the downstream part of the Meuse comprises the major part of this scene.

For the 1997 Oder flood, several ERS-2 SAR scenes were processed and used. The scene to which we refer in this paper covers the Polish-German border around Frankfurt-a-Oder (Germany) and Kostrzyn (Poland).

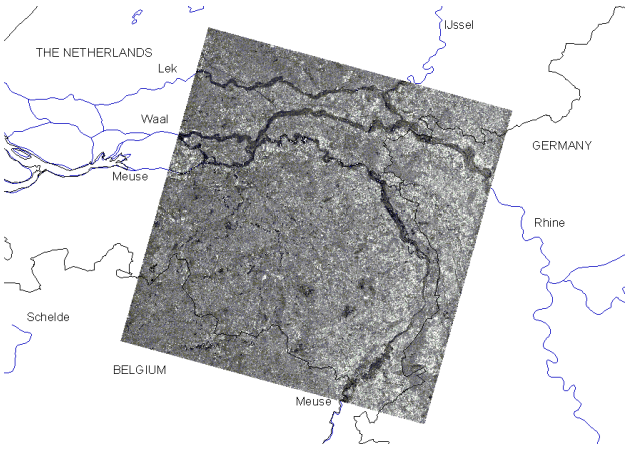

Figure 1. ERS1-SAR image of the Meuse and Rhine area, 31 January 1995.

3.2 Pre-processing

Before performing any analyses, the raw ERS-1 and ERS-2 data files were imported in Erdas/Imagine. The images were scaled down from 16 to 8 bits, using a standard deviation stretch. A median filter with a 7*7 pixel window size was used to reduce speckle. Because most of the middle Meuse scene consists of layover zones, a subset was created that contains only the area between the Belgian-Dutch border and Roermond. The images were then georeferenced using 1:50,000 topographical maps.

3.3 Image classification methods

To extract flooded areas, two methods were used, which are described below.

Supervised Classification. A supervised classification was performed on the images. First, training sites within the flooded and non-flooded parts of the image were digitised. The statistical distributions of pixel values in these training sites are the basis for the actual classification. A maximum

likelihood classification was then used to classify the images, assuming an approximately normal distribution of the pixel values within each class. Only two classes were used: 'flooded' and 'non-flooded'.

The resulting 'flooded area' classification typically results in many small groups of pixels that are classified as 'flooded'. Some of these small areas may actually be flooded (for example due to seepage or overland flow). However, many of them just result from the fact that discrimination between flooded and non-flooded areas is not always possible using SAR imagery. Similar results were reported by other authors (e.g. Oberstadler et al, 1997). Instead of applying spatial filtering or manual editing to improve the classification, a more automated approach was used. In many cases, the primary goal of a 'flooded area classification' is to derive flooded areas that are directly connected to the riverbed. When a GIS file with the locations of the main rivers is available, those areas can be derived relatively easily.

The method that was used here is shown schematically in figures 2 and 3. First, a 'clumping' operation is performed on the classified image. In the resulting output grid, each contiguous area (or 'clump') in the input grid is represented by a unique code. Secondly, an overlay operation is carried out which only keeps those clumps that are classified as 'flooded'. This 'flooded clumps' grid is then overlain with a grid with the locations of the main streams. This results in a table with the unique codes of the 'flooded' clumps intersected by a stream. This table is then used to recode the 'flooded clumps' grid, resulting in a grid that only contains the flooded areas adjacent to a stream.

Figure 2 *Improving the classified image by only keeping flooded areas that are connected to a stream*

As a final processing step, non-flooded 'gaps' within the flooded areas that are smaller than a user-defined number of pixels can be filled. This option is useful if the flooded areas on the radar image are very inhomogeneous, for example due to the presence of trees or buildings within the floodplains. The entire procedure was programmed in the Arc/Info macro language (AML), making it fully automated. Finally, the classification results of the two Meuse scenes were combined, resulting in a single flood map of the Dutch part of the Meuse catchment.

Figure 3 Schematic overview of the procedure to keep only the flooded areas that are intersected by a stream. See text for explanation.

The Snake method. The second method for the delineation of the flood boundary uses a statistical active contour technique (or snake). A dynamic curvilinear contour is used to search through the image space until it settles on feature boundaries (Horritt, 1999), aiming to identify the flood as a region of homogeneous speckle statistics. Rather than operating on a previously edge detected image like most snake techniques (Cohen, 1991, Williams and Shah, 1992, Mason et al., 1995), the statistical approach of Ivins and Porrill (1994) is used, whereby local image statistics are measured along the contour, reducing the effects of speckle but without loss of spatial resolution perpendicular to the contour. Curvature constraints are also included in the model to favour the production of a smooth contour and further reduce the effects of noise. The model is also capable of spawning smaller sub-snakes to represent a multiply connected region, and hence islands within the flood can be depicted. This image processing strategy can segment noisy images to within ~1 pixel (12.5m for ERS-1 and 2 SARs), when tested on synthetic imagery and when compared with a manual segmentation of a real SAR image.

Figure 4 shows an example of the algorithm applied to a ERS-2 SAR of the Oder 1997 flood. The snake was started as a narrow strip lying along the channel of the Oder, but diverted slighlty to include the area of flooded marshland to the right. For much of the river, the snake boundary coincides with that which would have been delineated manually, and the snake has ignored some regions of higher backscatter present in the main body of the flood. Problems appear for the region of marshland, however, where large areas of high backscatter (probably caused by wind roughening of the water surface) are evident. Although this roughening effect does affect other flooded areas, the greater fetch over the open marsh has increased the problem and generated a large area of high backscatter, which the snake identifies as unflooded.

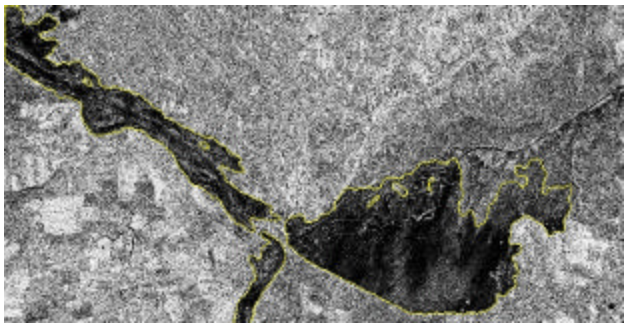

Figure 4 Flood Extent of the Oder flood of July 1997 near Kostrzyn (Poland), obtained using the Snake algorithm.

4. VALIDATION

4.1 Introduction

No direct water height or flood extent measurements were available to validate the results of the flooded area classification. However, some other data could be used for validation. First, detailed air photo – derived maps of the inundated areas of the 1993 and 1995 Meuse floods were available. Second, digitised maps with inundation classes could be obtained from the Dutch Water Authorities. Finally, the classification results were compared with the water classes in the CORINE land cover database.

4.2 Comparison with aerial photo interpretation

Detailed maps (scale 1:10,000) of the inundated areas –based on aerial photo interpretation- were obtained from the Meuse Water Authorities. They cover the Meuse region between Nijmegen and Eijsden (the border with Belgium). The photo's were first scanned and geometrically corrected using detailed topographic maps. The resulting images were then resampled to a pixel size of 12.5 meters. An automatic image classification was performed to 'translate' the different flooding classes (represented by different colours) into a meaningful GIS data layer. Visual inspection showed that some pixels were misclassified, mainly where text or line features were drawn on the map. Using a majority filter with a 3 by 3 pixel window size, most of these erroneous pixels could be removed. The few remaining erroneous pixels were removed by manual editing. The advantage of using a classified image over using a plain scanned map is, that with the former it is possible to perform all kinds of GIS analyses (e.g. overlaying, cross-tabulating with other GIS data etc.). Using only the plain scanned image, only a visual check would be possible. Because of the time involved in geometrically correcting the maps, it was decided to use only a small part of the Meuse catchment to validate the method. The area between Stein and Maastricht was chosen, because it encompasses a wide variety of land use types. Moreover, this area contains a relatively large proportion built-up area within the flooded zones, which would be expected to give difficulties with the SAR-classification. So, validating the method for this particular area should give a good impression of how the expected problems affect the classification results.

The results of the SAR-derived flood maps (hereafter referred to as SDF) and the air-photo interpretation (hereafter referred to as API) are shown in figure 5. Figure 5 shows that filling the non-flooded gaps results in a considerable improvement of the classification results. Table 1 shows the confusion matrix of the SDF and the API. Using the confusion matrix, several statistical measures were calculated to characterise the classification accuracy. First of all, the areas that are flooded on both the SDF and the API can be expressed as a percentage of the total area that is flooded on the API. This figure represents the percentage of actually flooded pixels (assuming that the API represents the 'absolute truth') that is also *classified* as being flooded. In remote sensing literature this is often referred to as 'producer's accuracy'. Alternatively, the area of correctly classified flooded pixels can be expressed as a percentage of the total area that is 'flooded' on the SDF. This is called the 'user's accuracy', and here it represents the percentage of 'flooded' pixels on the SDF that is actually flooded. In other words, it denotes the probability that a pixel is flooded, given that it is classified as being flooded (Richards, 1995). Needless to say, the same applies to the non-flooded areas.

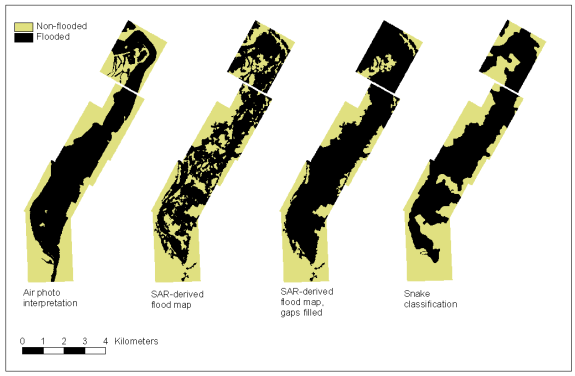

Figure 5. Comparison of the three different methods for flood extent derivation from SAR images with aerial photographs.

The table also gives the overall accuracy, which is simply the total percentage of correctly classified pixels. Finally, the accuracy is characterised by the KHAT statistic (Congalton, 1991; Lillesand & Kiefer, 1994), which takes into account the chance agreement between the reference data (here: the API) and the automated classifier. KHAT can be defined as:

The calculation of KHAT is explained here for the upper error matrix in table 1. The observed (overall) accuracy is simply the sum of the elements on the principal diagonal, divided by the grand total of the matrix (in this case, {(8.7 + 11.7)/27.7}). The *chance* agreement is the accuracy that we would get if the classification and the reference data were completely independent. To compute the chance agreement, the *expected* values on the principal diagonal have to be calculated. This is done by multiplying –for each element on the principal

diagonal- the marginal row and column totals, and dividing this product by the grand total. For example, to compute the expected union of the non-flooded areas, we would get {(12.1 × 12.6)/27.7} = 5.5 square kilometres. The expected values on the principal diagonal are then summed and divided by the grand total to get the chance agreement. In this example, the chance agreement equals {(5.5 + 8.5)/27.7} = 0.5. Using this value and the observed accuracy, it follows from the equation that KHAT equals 0.47.

Table 1 Validation of the SAR-derived flooded areas using aerial photo interpretation

a) Using SAR-derived flood map without filling gaps

	Aerial photo interpretation (API)		
	Non-flooded (sq.km)	Flooded (sq.km)	Total
Satellite-derived flood map (SDF)			
Non-flooded (sq.km)	8.7	3.9	12.6
Flooded (sq.km)	3.4	11.7	15.1
Total	12.1	15.6	27.7

Classification accuracy	% of API	% of SDF
Non-flooded	72	69
Flooded	75	78
Overall accuracy	74	
KHAT	0.47	

b) Using SAR-derived flood map with gaps filled

	Aerial photo interpretation (API)		
	Non-flooded (sq.km)	Flooded (sq.km)	Total
Satellite-derived flood map			
Non-flooded (sq.km)	8.0	1.0	9.1
Flooded (sq.km)	4.0	14.6	18.6
Total	12.1	15.6	27.7

Classification accuracy	% of API	% of SDF
Non-flooded	67	89
Flooded	93	78
Overall accuracy	82	
KHAT	0.62	

c) Using Snake classification (Matt Horritt)

	Aerial photo interpretation (API)		
	Non-flooded (sq.km)	Flooded (sq.km)	Total
Snake classification			
Non-flooded (sq.km)	9.3	2.6	11.9
Flooded (sq.km)	2.8	13.0	15.8
Total	12.1	15.6	27.7

Classification accuracy	% of API	% of SDF
Non-flooded	77	78
Flooded	83	82
Overall accuracy	81	
KHAT	0.60	

Looking at table 1, the computed accuracy values look reasonably high at first sight. However, using only two different classes, the probability of getting good classification results just by chance is very high. Consequently, the KHAT value is quite poor, despite the fair overall accuracy. The table shows that filling the non-flooded gaps in the flooded areas improves both the overall accuracy as well as KHAT (from 0.47 to 0.62). An adverse side effect of filling the gaps is that it results in a worse prediction of the *total* flooded and non-flooded areas: the 'gaps filled' classification overestimates the total area that is flooded. The snake method performs similar to the gaps-filled method and results in a KHAT of 0.60.

4.3 Comparison with inundation classes map

The classification results were also compared with maps of flood inundation frequency classes from the Meuse Water Authorities (figure 6, table 2). This map divides the winter bed of the Meuse into different zones, depending on their frequency of flooding. The definition of the different classes is related to the maximum discharge at Borgharen, which is used to estimate the return time of a flood. The following empirical formula is used:

)

Where:
T : return time (years)
Q : maximum discharge at Borgharen (m^3/s)
a, b : empirical constants.

The values for *a* and *b* have been revised several times. The most recent values are (Rijkswaterstaat, 1998):

a = 1297; *b* = 377.63 (*T* < 250)
a = 1476; *b* = 345.15 (250 < *T* < 10,000)

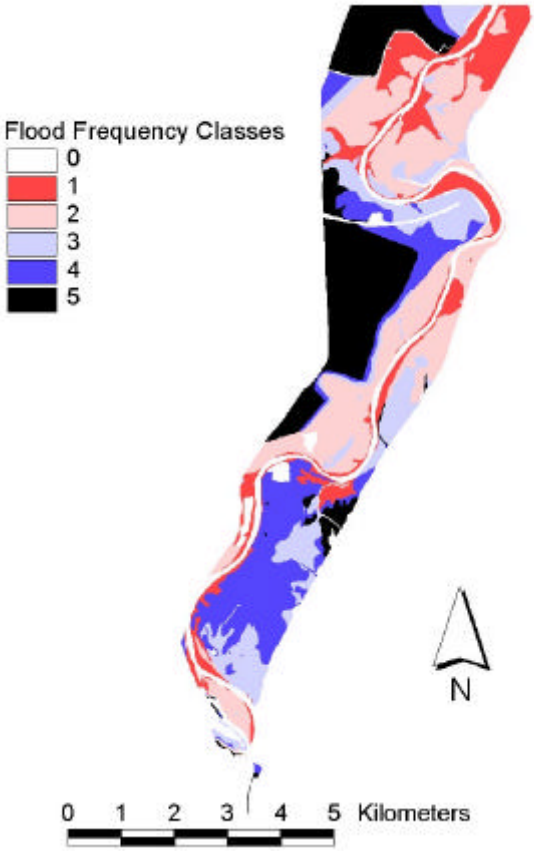

Figure 6. Flood inundation frequency classes of a part of the Meuse floodplain, the Netherlands.

Table 2 'Rijkswaterstaat' inundation classes

Inundation class	Discharge (m^3/s)	Return time (y) (RWS, 1978)	Return time (y) (RWS, 1998)
1	1500	2	1.7
2	2000	10	6.4
3	2500	50	24.2
4	3000	250	90.9
5	3800	3000	639.9

Table 2 gives the return time of each class according to these formulae (referred to as RWS 1998) as well as the values used on the original maps (RWS 1978). The maximum discharge of the 1995 flood in Borgharen was 2863 m^3/s, which yields an estimated return time of 63 years. Looking at table 2, this means that the area classified as 'flooded' should encompass

inundation classes 1, 2 and 3 in their entirety, as well as a part of class 4. No 'flooded' pixels should lie in class 5.

Table 3 shows that –as expected- large parts of the 'flooded' areas lie within classes 1, 2 and 3. However, especially in the case of the class 2 relatively large areas are occupied by 'non-flooded' pixels in the classification. Filling the 'non flooded' gaps in the classification improves the results. Also, about 20 % of the area in class 5 is classified as 'flooded', even though the actual flood was of a lower magnitude than assumed for this class. This could be due to errors in the inundation classes map or in the SAR-classification.

Table 3 Comparison of SAR-derived flooded areas with 'Rijkswaterstaat' inundation classes

a) Using SAR-derived flood map without filling gaps

Inundation class	Non-flooded (km²)	Flooded (km²)	Distribution non-flooded areas over inundation classes (%)	Distribution flooded areas over inundation classes (%)	% flooded area in each inundation class
1	7.7	43.0	0.2	22.7	84.8
2	16.9	43.7	0.3	23.1	72.1
3	17.6	18.0	0.4	9.5	50.5
4	21.0	13.3	0.4	7.0	38.7
5	42.2	10.0	0.9	5.3	19.1
n.a.	4761.6	61.1	97.8	32.3	1.3
Total:	4867.0	189.0	100	100	

b) Using SAR-derived flood map with gaps filled

Inundation class	Non-flooded (km²)	Flooded (km²)	Distribution non-flooded areas over inundation classes (%)	Distribution flooded areas over inundation classes (%)	% flooded area in each inundation class
1	4.0	46.6	0.1	22.1	92.1
2	11.6	48.9	0.2	23.1	80.8
3	13.1	22.5	0.3	10.6	63.2
4	18.8	15.6	0.4	7.4	45.3
5	41.0	11.2	0.8	5.3	21.5
n.a.	4756.2	66.6	98.2	31.5	1.4
Total:	4844.7	211.4	100	100	

'flooded' areas also belong to one of the inundation classes. This percentage is rather low. The main reason for this is that the summer bed of the river is not included in the flooding classes. Unfortunately, the digital version of the inundation classes map which was used for the analysis does not make any distinction between the river's summer bed and the areas that are never flooded: they both have the same code in the map. This is why more than 30 % of the 'flooded' areas do not belong to any inundation class. In future versions of these maps a distinction should be made between the summer bed and the areas that are never flooded.

5. APPLICATIONS OF A SAR-DERIVED FLOOD MAP

5.1 Introduction

In this section three applications of a SAR-derived flood map are presented. First, it is demonstrated how it can be used to derive land use statistics of the flooded areas. The second application shows how a SAR-derived flood map can be combined with a digital elevation model to estimate flooding depths.

5.2 Deriving land use statistics of the flooded areas

The SAR-derived flood map was combined with CORINE land use data (EEA, 1992). The CORINE land cover classes in the flooded areas are tabulated in table 4. Note that the 'gaps filled' classification was used to create this table, as it showed to be more accurate than the 'no gaps filled' classification. Not surprisingly, the results show that the flooded areas mainly consist of pasture and complex cultivation patterns. Figure 7 is a map with the main CORINE classes in the flooded areas along the Meuse river (January 1995). Figure 8 shows land use in flooded areas along the Oder river near Kostrzyn (Poland, July 1997).

Table 4 CORINE land use classes within flooded areas

CORINE class name	flooded (km2)	flooded (%)
Continuous urban fabric	6.1	2.9
Discontinuous urban fabric	1.1	0.5
Industrial or commercial units	0.9	0.4
Road and rail networks and associated land	0.2	0.1
Mineral extraction sites	2.2	1.0
Sport and leisure facilities	1.5	0.7
Non-irrigated arable land	18.6	8.8
Fruit trees and berry plantations	2.0	0.9
Pastures	72.6	34.3
Complex cultivation patterns	52.0	24.6
Mix agriculture and natural vegetation	4.2	2.0
Broad leaved forest	1.3	0.6
Coniferous forest	0.5	0.2
Mixed forest	1.7	0.8
Moors and heathland	0.2	0.1
Transitional woodland-scrub	0.4	0.2
Water courses	36.4	17.2
Water bodies	9.4	4.4
Total:	211.4	100

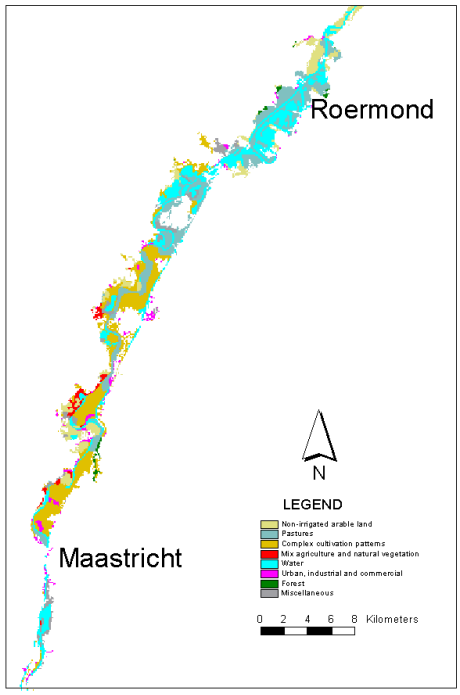

Figure 7. Land use in the flooded areas during the Meuse flood of January 1995.

5.3 Deriving flooding depths using a SAR-derived flood map

Another useful application of a SAR-derived flood extent map is to use it together with a high-resolution digital elevation model (DEM) to estimate flooding depths. Using stage-discharge relations, these flooding depths can then be used to estimate river discharge during a flood.

Theoretically, flooding depth could be determined by determining the height at the flood line (the edge of the flooded area) (Z_f). Then, for each pixel in the flooded area, the flooding

depth could be calculated by subtracting –for each pixel- the actual height (Z_i) from the height at the flood line.

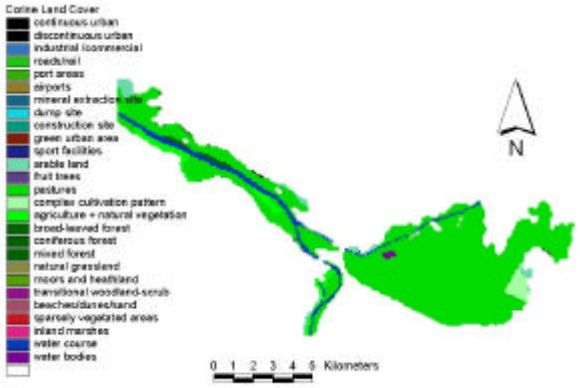

Figure 8 Land use in the flooded areas along the Oder river near Kostrzyn, Polish-German border, July 1997.

Actually, the situation is more complicated because the height of the flood line varies along the river channel because of gradient of the river. To overcome this problem, a method was developed that allows for local variation of the flood line height.

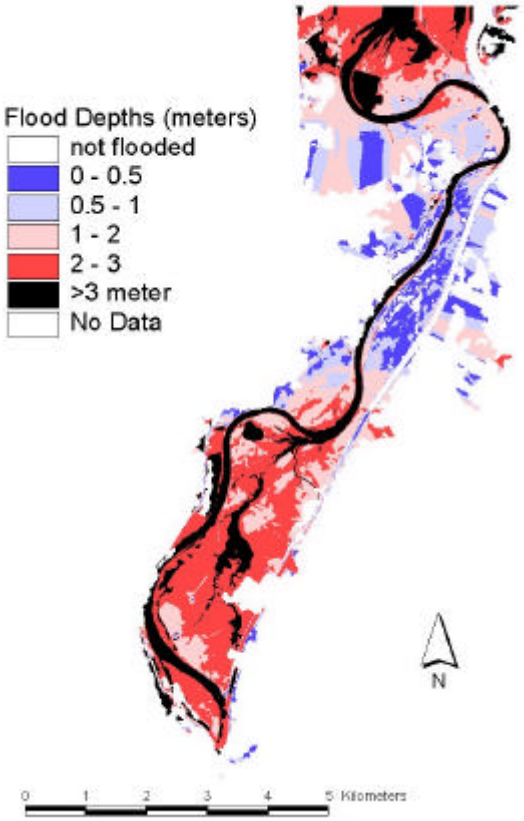

Figure 9 Flood depths in the Meuse floodplain during the flood on 31 January 1995, obtained by combining the SAR-flood extent map with a 5 m resolution DEM.

The flooding depths are determined by applying an edge filter on the 'gaps filled' classification to get the flood line. Then, the flood line is overlain with a digital elevation model to get the height at the flood line. To extend the flood line height over the flooded areas, a trend surface is fitted through the flood line heights. For each pixel the actual flooding depth is then calculated by subtracting the local height –which is determined from the DEM- from the local height of the flood line.

5.4 Validating 2-D Floodplain Simulation Models. The flood extent maps obtained by the SAR image classification can also be used to validate the flood extent simulated by 2-D hydrodynamic floodplain simulation models, as shown by Bates et al. (1997). The flood extent maps of the Meuse and Oder flood obtained here will be used in a later stage of the project to validate the flood extent simulated using the LISFLOOD simulation model (De Roo et al., 1999).

6. DISCUSSION AND CONCLUSIONS

Spaceborne SAR-imagery can be used to derive flooded areas. A semi-automatic method that uses the location of the main rivers to improve the classification results in a quick and straightforward way, is presented in this paper. Another method that was used is the 'Snake' algorithm developed by Horritt (1999). The methods were validated using aerial photo interpretation results, an inundation classes map and CORINE land use data. The comparison with the aerial photo interpretation shows an overall accuracy of over 80% for the 'gaps filled' classification and the snake method. Because a 'difficult' area was chosen to validate the results, it is expected that in most cases the method will actually perform better. Leaving the non-flooded gaps unfilled gives poorer results. The comparison with the digital inundation classes map proved to be difficult because it does not distinguish the river's summer bed as a separate class. The comparison with CORINE also gave difficulties because of CORINE's relatively coarse pixel size. Also, the geometric accuracy of CORINE is not satisfactory for making comparisons with narrow linear features like river beds.

Current experience with the methods used has also revealed some limitations and weak points that need further attention. First of all, the method discards any flooded areas not connected to the rivers in the 'streams' grid. So, detailed GIS layers with the locations of the streams have to be available. Problems can arise if a tributary stream that is visible in the radar image is not included in the streams layer (which is often the case when the 'streams' file is digitised using a small-scale map). The algorithm will discard any 'flooded' area in such a tributary that is not connected to the main stream.

Another limitation is that some flooded areas may lie well beyond the reach of any river, for example flooding due to seepage and rising groundwater. With the method used here, these areas would be discarded from the classification results.

A weak point of SAR imagery in general with respect to mapping flooded areas, is that it is unable to detect urban areas that are flooded. These areas generally appear as non-flooded gaps within the flooded areas. The ‘gap filling’ algorithm in the presented method provides a way to get around this problem, but it also results in an overestimation of the flooded areas. This problem may be overcome partly by fine-tuning the 'gap filling’ parameter in the algorithm. This parameter defines the minimum gap size for the non-flooded gaps: gaps that are smaller than this value are filled. Another solution may be to use digital elevation data. A possible approach would be to fill all gaps in the flooded areas initially. Using a detailed elevation model, the heights at the transition zone between the flooded and non-flooded areas could be used to estimate the flooding depth at each pixel. The estimated flooding depths could then be used to identify non-flooded islands within the flooded areas. However, also for this more accurate elevation models with a higher vertical and horizontal resolution are needed.

Another problem with spaceborne SAR imagery is the limited frequency of the available data. In the case of the ERS-2 satellite, the repetition rate is about 35 days. Although the actual frequency is higher because neighbouring orbits often partially show the same areas, floods may be ‘missed’ by the satellite (Portmann, 1997).

The final point that needs more attention is the geometric correction of the radar image that is necessary in order to apply the method. The geo-correction stage has shown to be the most time-consuming step in the entire image processing chain. Right now, each image is geometrically corrected using control points (e.g. road crossings) that are measured on 1:50,000 topographical maps. However, finding control points which are clearly visible on both the image and a 1:50,000 topographical map can be very difficult. A better approach could be to use – for each ERS-scene- one image as a ‘master’ and correct other images by fitting it onto this ‘master’ image. To ensure a sufficient spatial accuracy, the ‘master’ image should be geo-corrected very precisely, preferably using detailed topographical maps (scale 1:25,000 - 1:10,000).

Three applications of a SAR-derived flood map were presented. The combination with the CORINE land cover database results in land use statistics of the flooded areas. Combining the SAR-derived flood map with high resolution elevation data produces estimates of flooding depths. Finally, SAR derived flooded areas can be used to validate hydrodynamic floodplain flow models.

ACKNOWLEDGEMENTS

The high-resolution DEM, the flood inundation frequency maps and the aerial photographs of the Meuse 1995 flood were kindly made available by Mr. H. Bakker and Mr. L. Dekker of the Meuse Water Authorities in Maastricht (The Netherlands). Mr. R. Kidd , Mr G. Lemoine and Mr. S. Peedell of JRC-SAI are thanked for their advise on SAR, Erdas and ArcInfo.

REFERENCES

Badji, M., Dautrebande,S. 1997. Characterization of flood inundated areas and delineation of poor drainage soil using ERS-1 SAR imagery. Hydrological processes, 11, pp. 1441-1450.

Bates, P.D., Horritt, M.S., Smith, C.N., Mason, D.C. 1997. Integrating remote sensing observations of flood hydrology and hydraulic modelling. Hydrological Processes, 11, 1777-1795.

Cohen, L.D., (1991). On active contour models and balloons. CVGIP: Image Understanding, 53(2), 211-218.

Congalton, R.G. 1991. A review of assessing the accuracy of classifications of remotely sensed data. Remote sensing of environment 37, pp. 35-46.

Delmeire, S. 1997. Use of ERS-1 data for the extraction of flooded areas. Hydrological processes 11, pp 1393-1396.

De Roo, A.P.J., Wesseling, C.G., Van Deursen, W.P.A. 1999 Physically-based river basin modelling within a GIS: The LISFLOOD model. Special issue on Geocomputation. Hydrological Processes. In Press.

EEA, European Environment Agency Task-Force 1992. CORINE land cover. A European Community project presented in the framework of the international space year.

Horritt, M.S. 1999. A statistical active contour model for SAR image segmentation. Image and Vision Computing, 17, pp. 213-224.

Ivins, J. and Porrill, J. 1994. Statistical snakes: active region models. Image and Vision Computing, 13(5), pp. 431-438.

Lillesand, T.M. & Kiefer, R.W. Remote sensing and image interpretation. Wiley, London.

Mason, D.C. and Davenport, I.J. (1996). Accurate and efficient determination of the shoreline in ERS-1 images. IEEE Transactions on Geoscience and Remote Sensing, Vol 34, No 5, 1243-1253.

Oberstadler, R., Hönsch, H. & Huth, D. 1997. Assessment of the mapping capabilities of ERS-1 SAR data for flood mapping: A case study in Germany. Hydrological processes, 11, pp 1415-1425

Portmann, F. 1997. Hydrological runoff modelling by the use of remote sensing data with reference to the 1993-1994 and 1995 floods in the river Rhine catchment. Hydrological processes, 11, pp 1377-1392.

Richards, J.A. 1995. Remote sensing digital image analysis. An introduction (2nd edition). Springer-Verlag Heidelberg. 340 pp.

Williams, D.J. and Shah, M., (1992). A fast algorithm for active contours and curvature estimation. CVGIP: Image Understanding, 55(1), 14-26.